Langmuir

ARTICLE

pubs.acs.org/Langmuir

Wetting of a Drop on a Sphere

H. B. Eral,* G. Manukyan, and J. M. Oh

Physics of Complex Fluids, IMPACT and MESA+ Institute, Department of Science and Technology, University of Twente, P.O. Box 217, 7500 AE Enschede, The Netherlands

Supporting Information

ABSTRACT: In this work, the equilibrium morphology of a drop on a sphere is analyzed as a function of the contact angle and drop volume experimentally and with analytical effective interfacial energy calculations. Experimentally, a drop on a sphere geometry is realized in an oil bath by placing a water drop on a sphere coated with a dielectric, of which the radii of curvature are comparable with that of the drop. Electrowetting (EW) is used to change the contact angle of the water drop on the sphere. To validate the applicability of EW and the Lippman−Young equation on nonflat surfaces, we systematically investigate the response of the contact angle to the applied voltage (EW response) for various drop volumes and compared the results with the case of a planar surface. The effective interfacial energy of two competing morphologies, namely, the spherically symmetric "completely engulfing" and "partially engulfing" morphologies are calculated analytically. The analytical calculations are then compared to the experimental results to confirm which morphology is energetically more favored for a given contact angle and drop volume. Our findings indicate that the "partially engulfing" morphology is always the energetically more favorable morphology.

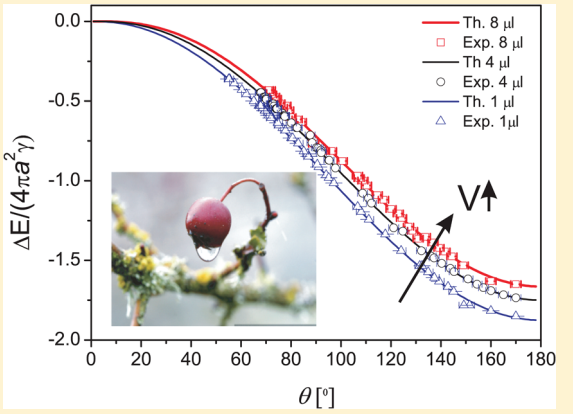

INTRODUCTION

Drops on curved surfaces are omnipresent in nature: dew drops on a spider web or raindrops on a spherical piece of fruit provide the most intriguing display of drop morphologies on curved surfaces (Figure 1). The morphology that a drop assumes on a curved surface is dictated by the wettability of the substrate, which is a key parameter in addressing fundamental problems of fluid stability on complex geometries.[1,2] The wettability of a substrate depends on the interplay between the contact angle and the geometry of the surface. For instance, a drop that partially wets a planar surface can engulf a fiber with the same wettability.

A drop on a sphere is not only a classical wetting geometry but is also often encountered in industrial and fabrication processes. Such processes can benefit from a fundamental understanding of the wettability of a drop on a sphere. Recently, this classical wetting geometry was evoked to synthesize complex colloidal particles by growing a colloidal particle inside a polymer drop. The colloidal particle that initially has a "completely engulfing" morphology later assumes a "partially engulfing morphology" as dictated by the wettability. The wettability of the polymer drop on the particle is controlled by reaction parameters such as the monomer concentration and temperature.[3,4] Various applications in colloidal science,[5] microfluidics,[6−10] detergency,[11] optofluidic lenses,[12] and electronic displays utilize spherical and other nonflat geometries.[13,14]

A drop on a sphere can have two topologically distinct morphologies: the partially engulfing morphology and the spherically symmetric completely engulfing morphology. These two morphologies are fundamentally different in terms of their symmetry and response to external driving forces such as shear and mechanical agitation. The wettability of a droplet on a spherical surface is addressed in various theoretical studies,[15−18] yet an experimental setup that allows precise control over parameters that determine the wettability and hence the equilibrium morphologies was missing. Previous experimental studies on spherical surfaces[19,20] utilized different materials to vary the contact angle. These methods do not offer a resolution that is sufficiently accurate to explore the range of contact angles defining the morphologies.

For the experimental realization of a drop on a sphere, a water drop in an oil bath is placed on a metal sphere coated with a dielectric layer. The wettability of the drop on the sphere is tuned by electrowetting (EW). Electrowetting is an efficient way of controlling the wettability of liquids on surfaces. The effective interfacial tension or equivalently the apparent contact angle θ of a conducting drop on a dielectric substrate is controlled by applying a potential difference (U) between the conducting liquid and an electrode integrated under the dielectric layer.[21] The difference between the cosine of the apparent contact angle θ and the cosine of the microscopic contact angle θ_Y at

Received: November 21, 2010
Revised: January 25, 2011
Published: April 05, 2011

ACS Publications © 2011 American Chemical Society

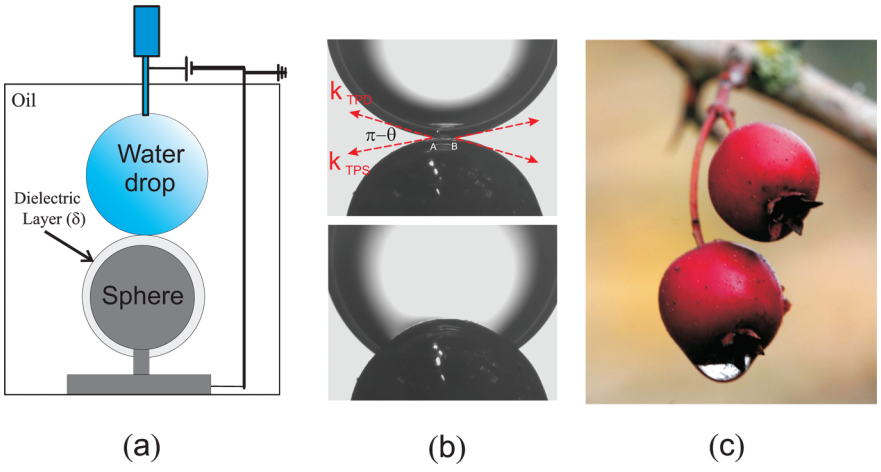

Figure 1. (a) Experimental setup consisting of a nonflat steel substrate coated with a dielectric layer of thickness δ and a water drop placed on the top, immersed in oil. The metal sphere is grounded, and the water drop is connected to a power supply in our setup. (b) Images of the experimental system where the voltage is changed from 0 to 300 V. (c) Partially engulfing morphology from nature, with a water drop sitting on a berry courtesy of S. Dreilinger. Note that in nature gravity is ever present as opposed to the experiments presented here, and it induces additional asymmetry.

the three-phase contact line (TCL) is proportional to the square of the applied potential (U^2) by the Lippmann−Young equation (eq 1)

$$\cos\theta = \cos\theta_Y + \eta, \eta \equiv \frac{\varepsilon_0\varepsilon_r U^2}{2\delta\gamma} \quad (1)$$

where θ_Y is the Young's angle and the electrowetting number η is defined by the vacuum permeability ε_0, the dielectric constant ε_r, the dielectric layer thickness δ, and the interfacial tension γ between liquid and solid phases.

First, we confirm the applicability of the Lippmann−Young equation and EW to study the equilibrium morphology of drops on curved surfaces. For this purpose, the response of the contact angle to the applied voltage (EW response) for a drop on a spherical, a cylindrical, and a planar substrate are compared. Drops on planar surfaces follow the Lippmann−Young relation (eq 1), and the applicability of this relation is confirmed for nonflat surfaces. Furthermore, we investigate the EW response on curved surfaces systematically as a function of the drop volume. The volume of the drop is varied to change the relative surface curvature (κ_1/κ_2), where κ_1 and κ_2 are the curvatures of the drop and surface, respectively.

The validation of the Lippmann−Young equation for nonflat surfaces is required because the intrinsic curvature of the geometry and the dielectric layer thickness influence the electric force distribution in the vicinity of the contact line. In the derivation of eq 1, the force distribution is obtained by assuming that the supporting substrate is flat. For a nonflat surface, the electrical force distribution is altered by the surface curvature, and as a consequence, the wettability change may deviate from the Lippmann−Young relation. Furthermore, this variation might depend on the relative surface curvature and dielectric layer thickness. It has been shown that the electrostatic force in the presence of electrowetting is concentrated near the contact line in a region on the order of the dielectric thickness.[22,23] From this point, one can hypothesize that the curvature of the sphere will not dramatically influence the EW response because of the large difference in dimensions considered. We provide experimental confirmation of this hypothesis, stating that the curvature effects can be ignored in this study.

Second, we determine the equilibrium shapes of a drop on a sphere experimentally and analytically by relying on the previous confirmation. The parameter space consisting of the contact angle and drop volume is scanned to find the stable morphologies with the experimental setup shown in Figure 1. The effective interfacial energies of the equilibrium morphologies are extracted experimentally by image processing and compared to analytical effective interfacial energy calculations. We believe that our systematic investigation will not only encourage further applications of EW to address fundamental wetting questions[24−26] where the manipulation of contact angle plays an important role in complex geometries[27−29] but also identify their limitations.

METHODS

Electrowetting Setup. Our buoyancy-neutral experimental setup consists of a stainless steel sphere (r = 1.5 mm) coated with a dielectric layer (the spatial variation of δ is between 2 and 4 μm with a mean of 3.1 μm) immersed in silicon oil (Fluka AS4 with density ρ = 1.01 g/cm^3 and viscosity μ = 6 mPa·s). The experiment is performed in oil to avoid evaporation and to reduce the contact angle hysteresis. The relative importance of gravity over interfacial tension is measured by the Bond number $Bo = \Delta\rho g L^2/\gamma$ where $\Delta\rho$ is the density difference between the oil and water phases and L is the characteristic length given by the radius of the drop with the maximum drop volume (8 μL). In our density-matched experimental setup $Bo \approx 10^{-2}$, in which the gravity effects can be ignored. A function generator (HP33250A) and an amplifier (Trek PZD350) are used to supply the required voltage. A video goniometer (OCA Dataphysics) is used to capture images. We place a water drop on top of the spherical substrates. The volume of the drop is controlled by an automated syringe pump whose needle also acts as an electrode (Figure 1). In these experiments, the volume of the drop (V_{drop}) is varied from 8 to 1 μL, which corresponds to the relative surface curvature κ_1/κ_2 variation from 0.6 to 5.

Substrate Preparation. Nonflat substrates are prepared with a cleaning procedure followed by two consecutive dip-coating steps. In the first step, the steel spheres are cleaned with ethanol in an ultrasonic bath for 15 min and left to dry in a fume hood under ambient conditions. Second, the substrates are dip coated with SU-8, the SU-8-coated substrates are placed on a hot plate for 3 min, and then the substrates are UV cured for 30 s. In the last step, the SU8-coated spheres are dip

dx.doi.org/10.1021/la104628q |*Langmuir* 2011, 27, 5340–5346

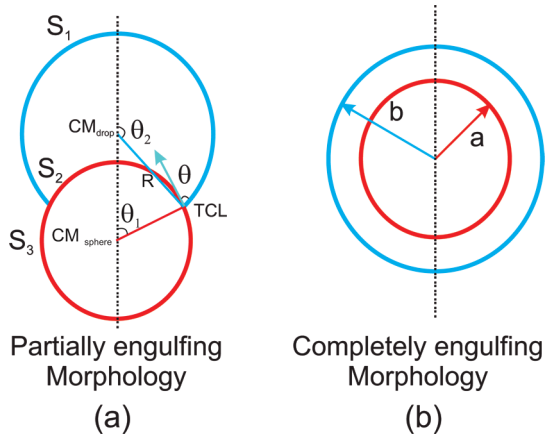

Figure 2. (a) Partially engulfing morphology and (b) completely engulfing geometry. The parameters indicated in the effective interfacial energy calculations are indicated in both panels.

coated again with a 0.6 wt % Teflon AF solution. The thickness of the dielectric layer is measured from scratched samples by scanning electron microscopy (SEM) after the experiments. The SEM images are given in the Supporting Information.

Analytical Effective Interfacial Energy Calculations. The effective interfacial energies of the two morphologies seen in Figure 2 are analytically calculated as a function of the drop volume and the contact angle. For this purpose, the radius of drop R in the partially engulfing morphology can be expressed in terms of a, θ_1, and θ_2 with the spherical shape assumption

$$R = \frac{\sin\theta_1}{\sin\theta_2}a \tag{2}$$

where θ is the contact angle, $\theta_2 = \theta + \theta_1$, and the radius of the spherical substrate is a. Then, the volume of the drop V_{drop} in the partially engulfing morphology is expressed as follows:

$$V = \frac{\pi}{3}[R^3(2 - 3\cos\theta_2 + \cos^3\theta_2) - a^3(2 - 3\cos\theta_1 + \cos^3\theta_1)] \tag{3}$$

The surface area of the drop (S_1), the drop−substrate contact area (S_2), and the air−substrate contact area (S_3) can be expressed as follows:

$$S_1 = 2\pi R^2(1 - \cos\theta_2) \tag{4}$$

$$S_2 = 2\pi a^2(1 - \cos\theta_1) \tag{5}$$

$$S_3 = 2\pi a^2(1 + \cos\theta_1) \tag{6}$$

The surface area of the drop (S_4) in contact with oil is given in completely engulfing morphology as

$$S_4 = 4\pi b^2 \tag{7}$$

where b is the radius of the drop in the completely engulfing morphology

$$b = \left(a^3 + \frac{V}{4\pi/3}\right)^{1/3} \tag{8}$$

There is a restriction on θ_1 when determining the equilibrium shape at a given drop volume.

$$\frac{\pi}{2} < \theta + \theta_1 < \pi \tag{9}$$

The difference $\Delta E = E_1 - E_2$ between the effective interfacial energy of the completely engulfed morphology (E_1) and the $\tilde{k}$ partially engulfed morphology (E_2) is given in eq 10

$$\Delta E = (S_4\gamma + (4\pi a^2)\gamma_{ws}) - (S_1\gamma + S_2\gamma_{ws} + S_3\gamma_{so}) \tag{10}$$

where γ, γ_{ws}, and γ_{so} denote the interfacial tension between the water and oil, water and solid, and solid and oil phases, respectively. The total effective interfacial energy can be rearranged as follows:

$$\frac{\Delta E}{\gamma} = (S_1 - S_4) + S_3\cos\theta \tag{11}$$

When $\Delta E < 0$, the partially engulfing morphology is the energetically favorable morphology in the parameter space spanned by the droplet V_{drop} and the contact angle θ, or else the completely engulfing morphology is the more stable morphology.

Image Processing. *Contact Angle Measurements.* Images of the drop on spherical substrates are captured with a CCD camera for different voltages and hence different contact angles. To measure the (apparent) contact angle θ on nonflat geometries (Figure 1b), a simple thresholding algorithm is used to locate the oil−water−sphere interface. The three-phase contact line (TCL) is detected on this interface. To measure the contact angle θ, two tangent vectors originating from the TCL are needed, one tangential to the drop−oil interface, $\tilde{k}_{TPD}$, and the other tangential to the spherical substrate−oil interface, $\tilde{k}_{TPS}$. Two vectors ($\tilde{k}_{TPD}$ and $\tilde{k}_{TPS}$) are defined by the least-squares fitting method in the vicinity of the TCL (Figure 1b). The angle $\pi-\theta$ between these two vectors gives us θ. The procedure was repeated for both sides of the TCL (A and B in Figure 1b), and the average contact angle is given in this study. The error in the contact angle measurements is calculated as 3 degrees by varying the parameters of the detection algorithm systematically.

Effective Interfacial Energy Calculations from Experimental Data. The effective interfacial energies of the two morphologies are calculated by extracting the surface areas of each interface from the digital images indicated in Figure 2. The partially engulfing morphology of three phases in contact (the oil−water drop interface area (S_1), the drop−substrate contact area (S_2), and the oil−substrate contact area (S_3)) is considered. For the completely engulfing morphology, the sphere is not in contact with the surrounding oil medium so only the oil−water drop interface and water−solid contact areas are considered.

The calculation of the effective interfacial energy for the completely engulfing morphology (E_1) requires the determination of water drop−solid sphere and water drop−solid contact areas. Because these contact areas are not contact-angle-dependent, provided that the drop volume and the radius of the sphere are known, E_1 can be calculated by multiplying the surface tension of the interfaces by the respective contact areas.

For the partially engulfing morphology, contact areas S_1, S_2, and S_3 vary with contact angle θ. E_2 varies with respect to θ, and the parameters that vary with respect to θ need to be identified to calculate E_2. The three parameters are θ_1, θ_2, and R as shown in Figure 2. Provided that the radius of the solid sphere (a) and the drop volume are known, parameters θ_1, θ_2, and R are calculated by a simple geometric relationship once the three-phase contact line (TCL) and the centers of the liquid drop CM_{drop} and sphere CM_{sphere} are known. More specifically, the images allow us to find CM_{drop} and CM_{sphere} precisely by fitting a circle to the contour of the drop and the sphere. θ-dependent θ_1 and θ_2 can be calculated from the inner product of two vectors. The inner product of the vector connecting CM_{drop} to CM_{sphere} and the vector connecting CM_{drop} to TCL gives θ_2. The inner product of the vector connecting CM_{drop} to CM_{sphere} with the vector connecting CM_{sphere} to TCL gives θ_1. These parameters allow for the calculation of contact areas S1, S2, and S3 from eq 6. Once the contact areas and the respective surface tension values are known, the effective interfacial energy for the partially engulfing geometry (E_2) is calculated.

The effective interfacial energies of two morphologies (E_1 and E_2) as a function of θ are later used in eq 11 to calculate the effective interfacial

dx.doi.org/10.1021/la104628q |*Langmuir* 2011, 27, 5340–5346

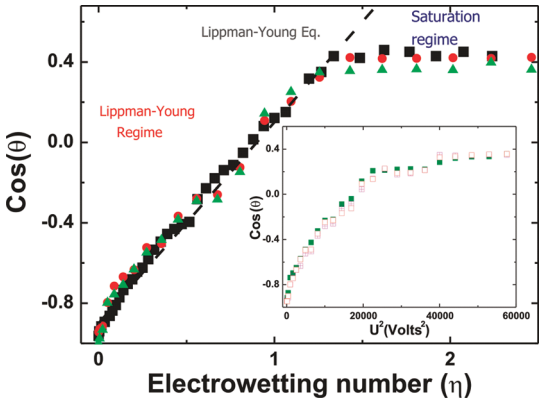

Figure 3. Influence of the substrate geometry and the drop volume on the response of the contact angle to an applied voltage (EW response). In the main panel, the cosine of the contact angle ($\cos\theta$) is plotted as a function of the EW number (η) for different geometries with a given drop volume ($V = 8\ \mu$L). The symbols indicate the substrate geometry: cylindrical (triangles), spherical (spheres), and flat (squares). The dashed line denotes the Lippmann−Young equation. In the inset, $\cos\theta$ is plotted as a function of U^2 for different drop volumes placed on a spherical geometry. The symbol fill patterns denote different drop volumes V_{drop}: (whole, 8 μL; empty, 4 μL; and crossed, 1 μL), respectively.

energy difference between the two morphologies, assuming that the spherical symmetry approximation holds (i.e., the drop shape is not disturbed by the wire and gravity).

RESULTS

To confirm the applicability of the Lippmann−Young equation for nonflat surfaces, we focus on two parameters: (a) substrate geometry and (b) drop volume. The responses of the contact angle with respect to the applied voltage for different substrate geometries and drop volumes are shown in Figure 3.

The influence of substrate geometry on the EW response is examined for a drop of 8 μL volume placed on spherical, cylindrical, and planar surfaces. Figure 3 demonstrates how the contact angle changes as a function of the applied voltage and compares the EW response for the aforementioned substrate geometries. The cosine of the contact angle ($\cos\theta$) is plotted as a function of the nondimensionalized EW number to account for variations in δ in Figure 3. δ is extracted from SEM images (Supporting Information). The curves follow the Lippmann−Young equation in the Lippmann−Young regime, followed by the saturation regime where the contact angle does not vary with applied voltage.[21]

All of the curves in Figure 3 collapse onto the Lippmann−Young equation prior to the saturation regime, implying that the influence of geometry on the EW response is negligible as previously hypothesized. The inset of Figure 3 displays the influence of the drop volume on the EW response on a spherical substrate. The contact angle ($\cos\theta$) is plotted against the square of the applied voltage for different drop volumes in the inset of Figure 3. The collapse of data for different drop volumes (denoted by symbol fill patterns in Figure 3) in the Lippmann−Young regime points out that the drop volume and hence the relative curvature have no influence on the response of the contact angle to the applied voltage for spherical substrates.

After validating the applicability of the Lippmann−Young equation and the reliability of EW on spherical substrates, we investigate the equilibrium morphologies of two morphologies by comparing the effective interfacial energies of the partially engulfing and the completely engulfing morphologies in Figure 2. To assess which morphology is more favorable, we calculate the effective interfacial energy difference between two morphologies (eq 10). When $\Delta E \geq 0$, the completely engulfing morphology is energetically favorable, and when $\Delta E \leq 0$, the partially engulfing morphology is energetically favorable.

The evaluation of the drop morphology as a function of the contact angle is monitored by plotting the projected distance $d(\theta)$ in two dimensions between the center of mass of the solid sphere CM_{sphere} and the center of mass of the drop CM_{drop} at a given contact angle in Figure 4a from the experimental images (Figure 4c). With increasing contact angle, $d(\theta)$ gradually decreases and the drop partially engulfs more of the sphere for all drop volumes. To characterize the equilibrium shapes for different drop volumes, we defined a symmetry parameter, λ, that denotes the relative distance $d(\theta)$ at a given contact angle normalized by the same distance at the Young's angle $d(\theta_Y)$ in eq 12. For a given contact angle, λ is determined from the experimental images as follows: the center of mass for the drop, CM_{drop}, and for the sphere, CM_{sphere}, are determined by identifying the contour of the drop−sphere via thrash holding and fitting a circle above and below the TCL. The distance between CM_{drop} and CM_{sphere}, $d(\theta)$, is determined for a given contact angle. The ratio of this distance at a given contact angle to this distance at the Young's angle, $d(\theta_Y)$, gives the symmetry parameter, eq 12. The inset schematic in Figure 4b demonstrates the symmetry parameter.

$$\lambda = \frac{d(\theta)}{d(\theta_Y)} \tag{12}$$

For $\lambda \cong 0$, the drop is in the completely engulfing morphology, and for $\lambda > 0$, the drop is in the partially engulfing morphology. Figure 4b demonstrates the variation of λ as a function of the contact angle (θ) for the aforementioned drop volumes. The curves of different drop volumes collapse onto a single curve, and none of the curves reach $\lambda = 0$, hence the partially engulfing morphology is always the preferred morphology.

The effective interfacial energy difference (ΔE) is calculated analytically and from experimental data as described in detail in the Methods section. Figure 5 shows the effective interfacial energy difference normalized by $4\pi a^2\gamma$ as a function of the contact angle for different drop volumes. The solid lines denote the analytical effective interfacial energy calculations whereas the discrete points indicate the effective interfacial energies calculated from the experimental data.

For all the effective interfacial energy calculations considered here, the effective interfacial energy difference indicates that the favorable morphology is the partially engulfing morphology irrespective of the drop volume and the contact angle. These results are in agreement with the effective interfacial energy analysis given in Figure 4. Only when the contact angles approach zero contact angle the energy difference converge to zero.

DISCUSSIONS

In the first part of the article, we investigated the applicability of the Lippmann−Young equation and the reliability of EW with

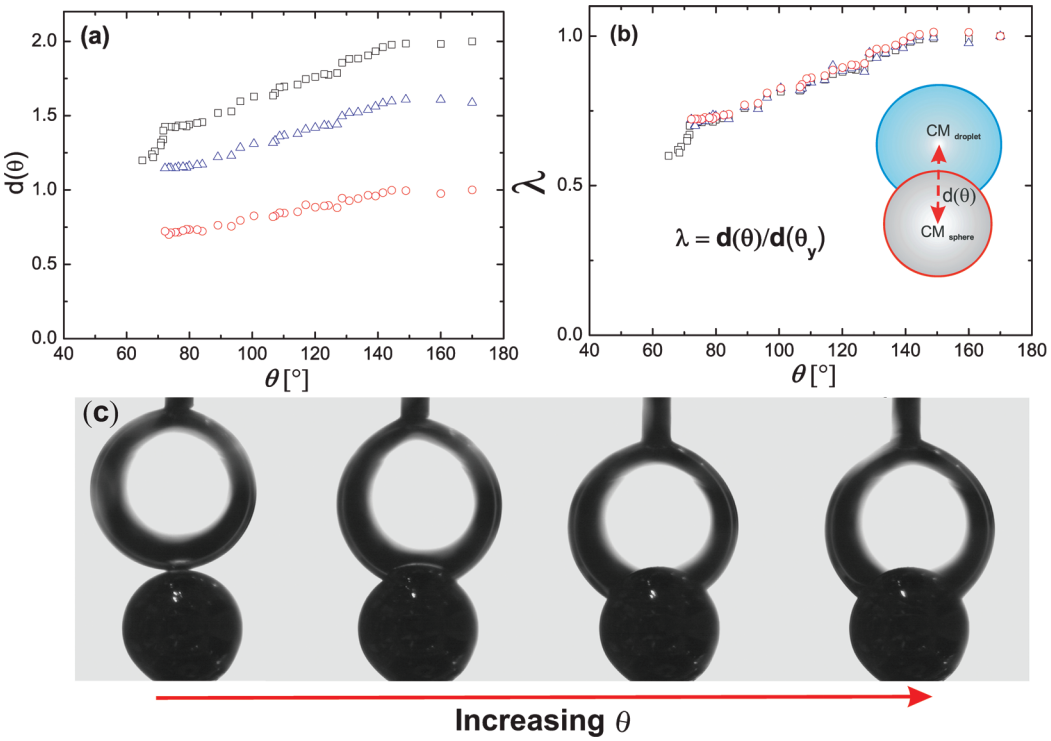

Figure 4. Evolution of the drop morphology as a function of drop volume V_{drop} and contact angle θ. (a) Distance between the center of mass of the drop and the sphere (θ) as a function of θ for different drop volumes. (b) Symmetry parameter (λ) vs θ. Different symbols correspond to different drop volumes (1 (○), 4 (Δ), and 8 μL (□)). The symmetry parameter (λ) is defined as the distance (θ) between the center of mass of the sphere and the drop at a given θ normalized by θ_Y, which is the distance when θ is equal to θ_Y. (Inset) θ and the symmetry parameter. (c) Overview of the experimental images for various θ values.

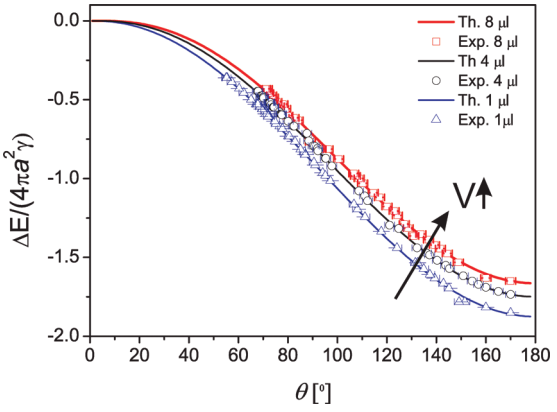

Figure 5. Normalized effective interfacial energy plotted as a function of contact angle for different drop volumes used in the experiment. Continuous lines indicate the theoretical effective interfacial energies and discrete points of same color indicate the experimental effective interfacial energies extracted from image processing. Different symbols correspond to different drop volumes (1 (○), 4 (Δ), and 8 μL (□)).

respect to drop morphology analysis on curved surfaces by varying two parameters: substrate geometry and drop volume. Figure 3 confirms the applicability of the Lippmann−Young equation to nonflat geometries as well as flat geometries in the Lippman−Young regime. Hence the effect of the geometry and the relative curvature in our experimental parameter space can be ignored. We have also looked at the influence of drop conductivity on the EW response for spherical substrates. The dependence of the EW response on drop conductivity is found to follow similar behavior as on a planar surface[30−32] (details in Supporting Information). In Figure 3 and its inset, a slight scattering and deviation from the Lippmann−Young equation are observed. This is attributed to a spatial variation in the dielectric layer thickness of samples used in experiments that we have identified to vary between 2 and 5 μm.

Finally, the effective interfacial energy difference (ΔE) between the two morphologies is calculated analytically and from the experimental data in Figure 5. ΔE always lies in the negative region, indicating that the partially engulfing morphology is the favored morphology irrespective of the drop volume and the contact angle. At zero contact angle, the effective interfacial energy of the two competing morphologies becomes identical, which means that the surface energy of the wetted area is the same as that of the nonwetted area ($\gamma + \gamma_{sw} = \gamma_{so}$). Because of contact angle saturation phenomena, very low contact angles cannot be reached experimentally, yet the analytical effective interfacial energy calculations show that the two morphologies have equally effective interfacial energies, indicating that the two morphologies are equally favorable to a zero contact angle. It implies that with large enough drops and a zero contact angle a transition from one morphology to the other is theoretically possible.

In this study, the upper and lower bounds of drop volume considered are defined by the limitations of the experimental setup and the associated physics. The smallest volume utilized is bound by the size of the wire in a conventional EW setup (the drop diameter has to be a lot larger than the wire). The upper limit is bound by the capillary limit. Provided that we are not

dx.doi.org/10.1021/la104628q |Langmuir 2011, 27, 5340–5346

limited by the experimental parameters, these two extreme limits may provide interesting insights. For the generality of our results, it is relevant to discuss these extreme cases: when (i) the drop volume V_{drop} is much larger than the volume of the sphere V_{sphere} (i.e., when $V_{drop} \gg V_{sphere}$) and (ii) when $V_{drop} \ll V_{sphere}$, which is the other extreme. In case i, from the effective interfacial energy calculations we can deduce that the larger the ratio of V_{drop} to V_{sphere}, the smaller the difference ΔE. This points out that the effective interfacial energies of two states become comparable at all contact angles. In other words, ΔE versus the θ landscape approaches the $\Delta E = 0$ line (i.e., less energy is required to jump from one morphology to the other upon application of flow or mechanical agitation). For case (ii), the transition becomes rather difficult and the systems resemble the flat geometry.

The major source of error in the calculation of the effective interfacial energy from experiments is the determination of the contact angle in image processing. The error in the measurement is within 3°. Because the experimental and theoretical values collapse for all of the drop volumes, effects that deform the drop such as contact angle hysteresis, gravity, and the wire are not significant.

Utilizing EW to study fundamental wetting problems in complex geometries provides unmatched control over the contact angle, yet the limitations in EW should not be neglected. The contact angle saturation does not allow contact angles smaller that 35° to be reached. This limitation can be avoided by evoking an inverse EW scheme where a water drop is immersed in oil yet must be identified as a limitation of the method.[28] Conventional and inverse EW schemes can be used in parallel to reach larger contact angle ranges. Special care has to be taken for the conventional EW setup that we utilized because the wire has to be much smaller than the drop to minimize its effect on the symmetry of the system. Interdigitated electrode or inverse EW setups can be evoked to bypass this effect. In our study, we monitored the symmetry of the drop and manually interfered by moving the wire when the symmetry was compromised.

Our results demonstrate the wetting behavior of a liquid drop on a spherical surface. Comparing this behavior to the wettability of a liquid drop on an infinitely long cylindrical fiber points to some interesting differences. Fibers can be fully engulfed with a nonzero contact angle, where the contact angle has to be infinitesimally small with respect to a drop on a sphere for complete engulfment.[11,28,33] The critical contact angle, at which a drop engulfs a fiber, depends on the drop volume, whereas for a drop on a sphere such a critical contact angle is not drop-volume-dependent. From a topological point of view, the partially engulfing morphology is a singly connected topology once the drop engulfs the sphere, and spherical symmetry is established. For a fiber, asymmetric morphology is singly connected, and the symmetric morphology is multiply connected. This topological difference is one of the underlying physical reasons that the wetting behaviors of the two geometries are different.

CONCLUSIONS

In this work, we first validated EW as a tool for studying wetting problems of nonflat geometries. Later, relying on this validity, we confirmed the equilibrium morphologies of a classical wetting geometry: a drop on a sphere as a function of governing variables such as drop volume and contact angle, experimentally and analytically.

For validation purposes, the influence of substrate geometry on the EW response is studied systematically by considering the effect of the drop volume and hence the relative curvature. For different drop volumes corresponding to different relative drop-to-substrate curvatures, the EW response stayed the same, indicating that in the experimental parameter regime covered, curvature effects can be ignored. Comparing the response of the contact angle to the EW number (η) for flat, cylindrical, and spherical geometries, we conclude that the substrate geometry has no influence on the EW response. Our results indicate that the Lippmann−Young equation holds for spherical substrates as in flat substrates within the experimental parameters examined. Furthermore, we hypothesize that the effect of substrate curvature can be ignored for cases where the dielectric layer thickness is much smaller that the characteristic dimension of the geometry such as the radius of curvature of the surface ($\delta \ll \kappa_2$).

Relying on applicability of EW on nonflat surfaces, we studied the equilibrium morphologies of two competing geometries by calculating the effective interfacial energy of both morphologies analytically and experimentally. Our results show that the partially engulfing morphology is energetically more favorable and the mechanically stable morphology as the absolute effective interfacial energy of the engulfing morphology is greater that the partially engulfing morphology under all conditions. Only for vanishing contact angles the effective interfacial energy of the completely engulfing morphology is comparable to the partially engulfing morphology. It is noteworthy to mention that the application of EW to wetting problems in complex geometries opens pathways to explore industrially relevant problems such as the mechanical stability of liquid bridges between nonflat geometries such as spheres or fibers.

ASSOCIATED CONTENT

Supporting Information. Influence of geometry on contact angle as a function EW number (η). SEM of the surfaces scratched after the experiment for the determination of the dielectric layer thickness. This material is available free of charge via the Internet at http://pubs.acs.org.

AUTHOR INFORMATION

Corresponding Author
*E-mail: h.b.eral@utwente.nl.

ACKNOWLEDGMENT

We thank the NWO for funding this research, A. Staicu for early experiments, B. M. Mognetti for fruitful discussions, K. Smit for mechanical assistance, and C. Aran and M. Bikel of the MTG group at the University of Twente for SEM images.

REFERENCES

(1) de Gennes, P.; Brochard-Wyart, F.; Quere, D. *Capillarity and Wetting Phenomena: Drops, Bubbles, Pearls, Waves*; Springer: New York, 2004.

(2) Plateau, J. *Statique Experimentale et Theorique des Liquides Soumis aux Seules Forces Moleculaires*; Gauthier-Villars: Paris, 1873.

(3) Mock, E. B.; De Bruyn, H.; Hawkett, B. S.; Gilbert, R. G.; Zukoski, C. F. Synthesis of anisotropic nanoparticles by seeded emulsion polymerization. *Langmuir* **2006**, *22*, 4037.

(4) Kraft, D. J.; Vlug, W. S.; van Kats, C. M.; van Blaaderen, A.; Imhof, A.; Kegel, W. K. Self-assembly of colloids with liquid protrusions. *J. Am. Chem. Soc.* **2009**, *131*, 1182.
(5) Eral, H. B.; van den Ende, D.; Mugele, F.; Duits, M. H. G. Influence of confinement by smooth and rough walls on particle dynamics in dense hard-sphere suspensions. *Phys. Rev. E* **2009**, *80*, 061403.
(6) Psaltis, D.; Quake, S.; Yang, C. Developing optofluidic technology through the fusion of microfluidics and optics. *Nature* **2006**, *442*, 381.
(7) Cho, S. K.; Moon, H.; Kim, C.-J. Creating, transporting, cutting, and merging liquid droplets by electrowetting-based actuation for digital microfluidic circuits. *J. Microelectromech. Syst.* **2003**, *12*, 70.
(8) Mognetti, B. M.; Yeomans, J. M. Capillary filling in microchannels patterned by posts. *Phys. Rev. E* **2009**, *80*, 056309.
(9) Mognetti, B. M.; Yeomans, J. M. Using electrowetting to control interface motion in patterned microchannels. *Soft Matter* **2010**, *6*, 2400.
(10) Eral, H. B.; Oh, J. M.; van den Ende, D.; Mugele, F.; Duits, M. H. G. Anisotropic and hindered diffusion of colloidal particles in a closed cylinder. *Langmuir* **2010**, *26*, 16722.
(11) Carroll, B. Physical aspects of detergency. *Colloids Surf., A* **1993**, *74*, 131.
(12) Heikenfeld, J.; Zhou, K.; Kreit, E.; Raj, B.; Yang, S.; Sun, B.; Milarcik, A.; Clapp, L.; Schwartz, R. Electrofluidic displays using Young-Laplace transposition of brilliant pigment dispersions. *Nat. Photonics* **2009**, *3*, 292.
(13) Zhou, K.; Heikenfeld, J. Arrayed electrowetting microwells. *Appl. Phys. Lett.* **2008**, *92*, 113515.
(14) Chen, J. Electrowetting-actuated zoom lens with spherical-interface liquid lenses. *J. Opt. Soc. Am. A* **2008**, *25*, 2644.
(15) Hołyst, R.; Poniewierski, A. Wetting on a spherical surface. *Phys. Rev. B* **1987**, *36*, 5628.
(16) Upton, P. J.; Indekeu, J. O.; Yeomans, J. M. Wetting on spherical and cylindrical substrates: global phase diagrams. *Phys. Rev. B* **1989**, *40*, 666.
(17) Hadjiagapiou, I. A. Wetting on a spherical-shell substrate. *J. Phys. Chem. B* **1997**, *101*, 8990.
(18) Stewart, M. C.; Evans, R. Wetting and drying at a curved substrate: long-ranged forces. *Phys. Rev. E* **2005**, *71*, 011602.
(19) Extrand, C. W.; Moon, S. I. Contact angles on spherical surfaces. *Langmuir* **2008**, *24*, 9470.
(20) Mason, G.; Clark, W. Liquid bridges between spheres. *Chem. Eng. Sci.* **1965**, *20*, 859–866.
(21) Mugele, F.; Baret, J. Electrowetting: from basics to applications. *J. Phys.: Condens. Matter* **2005**, *17*, 705–744.
(22) Mugele, F.; Buehrle, J. Equilibrium drop surface profiles in electric fields. *J. Phys.: Condens. Matter* **2007**, *19*, 375112.
(23) Buehrle, J.; Herminghaus, S.; Mugele, F. Interface profiles near three-phase contact lines in electric fields. *Phys. Rev. Lett.* **2003**, *91*, 086101.
(24) Callies, M.; Quere, D. *Soft Matter* **2005**, *1*, 51.
(25) Herminghaus, S.; Brinkmann, M.; Seemann, R. Wetting and dewetting of complex surface geometries. *Annu. Rev. Mater. Res.* **2008**, *38*, 101.
(26) Borkent, B. M.; de Beer, S.; Mugele, F.; Lohse, D. On the shape of surface nanobubbles. *Langmuir* **2010**, *26*, 260.
(27) Brinkmann, M.; Lipowsky, R. Wetting morphologies on substrates with striped surface domains. *J. Appl. Phys.* **2002**, *92*, 4296.
(28) Eral, H. B.; de Ruiter, J.; de Ruiter, R.; Oh, J. M.; Semprebon, C.; Brinkman, M.; Mugele, F. Drops on functional fibers: from barrels to clam shells and back. *Soft Matter*, **2011**; DOI:10.1039/C0SM01403F.
(29) Baret, J.-C.; Decra, M.; Herminghaus, S.; Seemann, R. Electro-actuation of fluid using topographical wetting transitions. *Langmuir* **2005**, *21*, 12218.
(30) Jones, T. B.; Fowler, J. D.; Chang, Y. S.; Kim, C.-J. Frequency-based relationship of electrowetting and dielectrophoretic liquid micro-actuation. *Langmuir* **2003**, *19*, 7646.
(31) Jones, T. B. On the relationship of dielectrophoresis and electrowetting. *Langmuir* **2002**, *18*, 4437.
(32) Kang, K. H. How electrostatic fields change contact angle in electrowetting. *Langmuir* **2002**, *18*, 10318.
(33) Carroll, B. Equilibrium conformations of liquid drops on thin cylinders under forces of capillarity. A theory for the roll-up process. *Langmuir* **1986**, *2*, 248.